FFI RAPPORT

$ZnGeP_2$-BASED OPTICAL PARAMETRIC OSCILLATOR FOR 8-11 µm GENERATION

NICOLAS Stephane, ARISHOLM Gunnar, LIPPERT Espen,
STENERSEN Knut, RUSTAD Gunnar

FFI/RAPPORT-2004/04129

$ZnGeP_2$-BASED OPTICAL PARAMETRIC OSCILLATOR FOR 8-11 μm GENERATION

NICOLAS Stephane, ARISHOLM Gunnar, LIPPERT Espen, STENERSEN Knut, RUSTAD Gunnar

FFI/RAPPORT-2004/04129

FORSVARETS FORSKNINGSINSTITUTT
Norwegian Defence Research Establishment
P O Box 25, NO-2027 Kjeller, Norway

FORSVARETS FORSKNINGSINSTITUTT (FFI)
Norwegian Defence Research Establishment

P O BOX 25
N0-2027 KJELLER, NORWAY

UNCLASSIFIED

SECURITY CLASSIFICATION OF THIS PAGE
(when data entered)

REPORT DOCUMENTATION PAGE

1) PUBL/REPORT NUMBER	2) SECURITY CLASSIFICATION	3) NUMBER OF PAGES
FFI/RAPPORT-2004/04129	UNCLASSIFIED	36
1a) PROJECT REFERENCE	**2a) DECLASSIFICATION/DOWNGRADING SCHEDULE**	
FFI-III/856/914	-	

4) TITLE

$ZnGeP_2$-BASED OPTICAL PARAMETRIC OSCILLATOR FOR 8-11 μm GENERATION

5) NAMES OF AUTHOR(S) IN FULL (surname first)

NICOLAS Stephane, ARISHOLM Gunnar, LIPPERT Espen, STENERSEN Knut, RUSTAD Gunnar

6) DISTRIBUTION STATEMENT

Approved for public release. Distribution unlimited. (Offentlig tilgjengelig)

7) INDEXING TERMS

IN ENGLISH:	IN NORWEGIAN:
a) Optical parametric oscillators	a) Optiske parametriske oscillator
b) Nonlinear optics	b) Ikke-lineær optikk
c) Infrared sources	c) Infrarøde kilder
d) Optical materials	d) Optiske materialer
e)	e)

THESAURUS REFERENCE:

8) ABSTRACT

Operation of a $ZnGeP_2$-based optical parametric oscillator (OPO) for generation of 8-11 μm radiation is studied. The primary source used to pump the OPO is a KTP-based OPO pumped by a Nd:YAG laser, giving up to 2 mJ pump energy at 2.07 μm at 20 Hz pulse rate. A conversion efficiency of 9% is obtained at 8 μm, with a beam quality M^2 of 2.4-3. Wavelength tuning in the 8-11 μm range and simultaneous oscillation of two signal/idler pairs is demonstrated. Length matching effects between the OPO and the pump source are also observed. Simulations of the OPO show good agreement with the experimental results in general, but some discrepancies were noticed.

9) DATE	AUTHORIZED BY This page only	POSITION
2004-11-29	Johnny Bardal	Director

ISBN 82-464-0897-6

UNCLASSIFIED

SECURITY CLASSIFICATION OF THIS PAGE
(when data entered)

CONTENTS

Page

$ZnGeP_2$-BASED OPTICAL PARAMETRIC OSCILLATOR FOR 8-11 μm GENERATION

1 INTRODUCTION

Military applications, such as electro-optic countermeasures, require tunable laser sources in the 3-5 μm and 8-12 μm infrared atmospheric transmission windows. It has proven to be difficult, however, to build efficient lasers that can cover these wavelength regions. The most attractive solution to this problem is to use optical parametric oscillators (OPOs), which can convert the radiation from near infrared primary laser sources to the desired regions. The nonlinear optical properties of zinc germanium phosphide (ZGP) make this material suitable for this purpose. It has a large non-linear coefficient, a broad optical transparency range from 2 μm to 11 μm, and a large thermal conductivity. OPOs based on ZGP are the prime choice for conversion of 2 μm primary radiation to the 3-5 μm band [1]. Such OPOs can also be used for conversion to the 8-11 μm band, but there are only few reports on ZGP-based OPOs used to reach this band [2, 3].

The purpose of this work is to study a 2 μm pumped ZGP-based OPO for generation of tunable radiation in the 8-11 μm band. In the next chapter the theory for OPOs is briefly reviewed. The experimental layout and the optical components are described in Chapter 3, the simulation model is presented in Chapter 4, and experimental results, as well as comparison with simulations, are given in Chapter 5.

2 THEORY

Extensive treatments of the theoretical background for nonlinear optics and OPOs can be found in [4-6]. In this chapter, we will briefly discuss singly and doubly resonant OPOs and introduce the concept of length matching the OPO to the pump laser.

2.1 Optical Parametric Oscillation

The OPO is composed of a second order nonlinear optical medium placed inside an optical resonator. The incoming beam at the frequency ω_3 is called the pump beam. The two generated beams at ω_1 and ω_2 (with $\omega_1 \leqslant \omega_2 < \omega_3$) are usually called the idler and signal beams, respectively (see Figure 2.1). The conversion efficiency of an OPO depends on the intensities of the three interacting beams. Large intensity values of the signal and/or idler can be obtained with the optical resonator. The OPO is said to be a doubly resonant oscillator (DRO) if the optical resonator is resonant for both signal and idler. Likewise, if only the signal or the idler is resonant, the OPO is said to be a singly resonant oscillator (SRO).

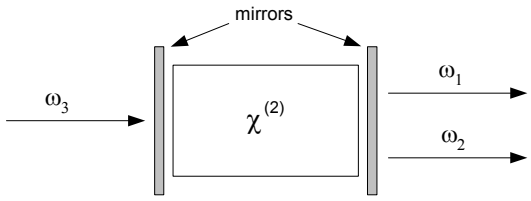

Figure 2.1. Optical parametric oscillator.

The coupled-wave equations show that the energy transfer direction depends on the relative phase between the beams [4, 6]. In the case of a SRO, the non-resonant signal or idler can adapt its phase to maximise the conversion efficiency. SROs are therefore not phase sensitive, but require normally higher pump intensity to reach threshold than DROs. DROs, on the other hand, have significantly lower pump threshold energy, but since they are phase sensitive, variations in the resonator length or pump phase can result in output fluctuations of the OPO. If the gain is low, e.g. in CW OPOs, the effect of phase variations is particularly strong, and active stabilisation of the resonator length may be necessary. With high gain, on the other hand, the phase tolerance is greater and DROs can work well even without stabilisation. The system studied in this work is very close to a SRO.

2.2 Length Matching

The optical resonator is often made as short as possible to minimise the build-up time of the signal and idler and the pump threshold energy, and thereby maximise the conversion efficiency. However, we have previously shown that, in case of a DRO pumped by a multi-longitudinal-mode (MLM) and quasi-periodic pump, the output energy can be increased by matching the resonator length of the OPO with that of the MLM pump source [1, 7]. In this case, the signal and idler beams interact with approximately the same pump phase and amplitude at each round-trip, as they do with a single-longitudinal-mode pump source. It results in higher conversion efficiency compared to if they interact with a random pump phase and amplitude at each round-trip. SROs are not phase sensitive, and the length matching effect is therefore expected to be weaker, as predicted by numerical simulations [7]. In Section 5.5, we have verified the SRO length matching effect experimentally.

3 EXPERIMENTAL LAYOUT

The experimental set-up is sketched in Figure 3.1. It consists of a pump source, the ZGP–based OPO, a monochromator for spectral measurements, and a pyroelectric camera to characterise the beam. The output energy from the ZGP OPO is measured by placing a power meter E_1 in the laser beam path. The present chapter describes the different components of the experimental set-up. The ZGP OPO itself is described thoroughly in Section 3.2.

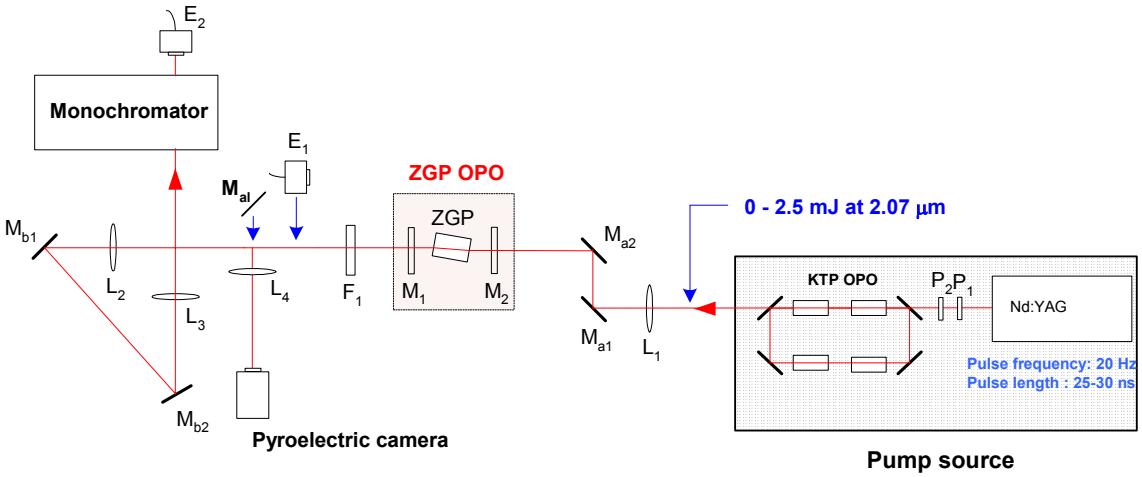

Figure 3.1. Experimental set-up of the ZGP-based OPO. L_1, L_2, L_3, L_4 – lenses, M_1, M_2, M_{a1}, M_{a2}, M_{b1}, M_{b2}, M_{al} – mirrors, F_1 – filter, E_1, E_2 – power meter. The pump beam diameter is about 800 µm ($1/e^2$ – diameter) in the ZGP crystal. The filter F1 transmits only the idler (8 – 12 µm). The beam shape is captured with the pyroelectric camera, and the spectrum is measured with the monochromator. The output energy is measured with the power meter E_1. The half-waveplate P_1 combined with the polariser P_2 allows regulation of the pump power.

3.1 Pump source

The pump source is a KTP-based ring OPO pumped by a diode-pumped Q-switched Nd:YAG laser [8]. This laser emits 25-30 ns pulses at 1064 nm, with 20 Hz pulse rate, beam quality $M^2 \approx 1.5$, and 15-20 GHz (FWHM) spectral width. The KTP OPO emits two beams with orthogonal polarizations at 2.07 µm and 2.17 µm, as shown in Figure 3.2. The maximum available pulse energy at 2.07 µm is 2.5 mJ/pulse, and the spectral bandwidth is ≈ 100 GHz. M_{a1} and M_{a2} are highly reflective for the signal (at 2.07 µm) and transmit the idler (at 2.17 µm).

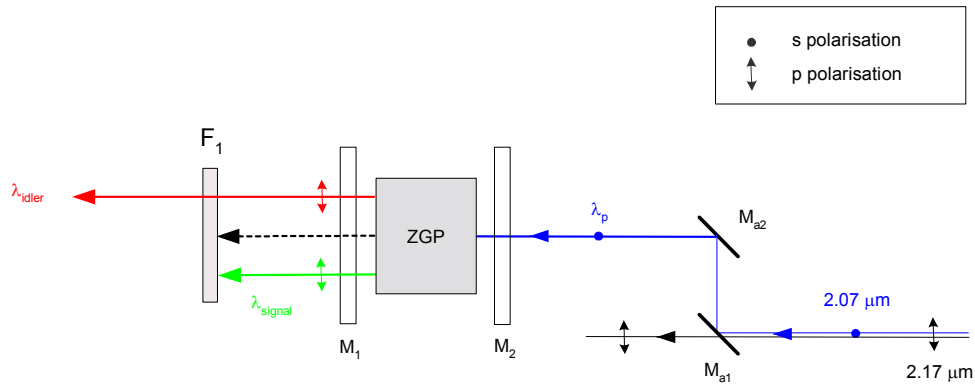

Figure 3.2. Beam polarisations in the ZGP-based OPO.

The ZGP-based OPO is pumped by the 2.07 µm output beam. The 300 mm focal length lens *L1* is AR-coated at 2 µm and focuses the pump beam into a 800 µm $1/e^2$ diameter spot in the ZGP crystal (see Figure 3.3). It has a beam quality factor M^2 of about 1 and 1.2 for the vertical and horizontal directions, respectively, and is slightly astigmatic, as shown by Figure 3.3.

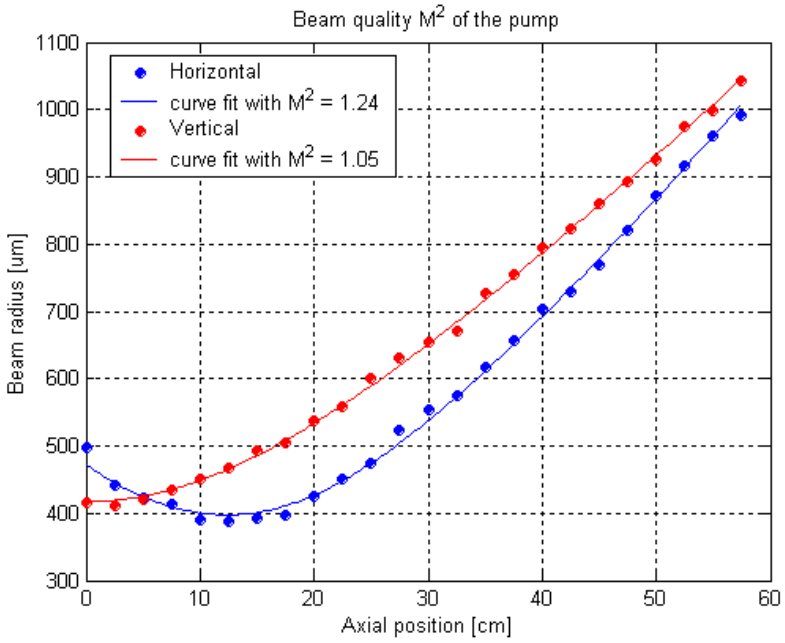

Figure 3.3. Beam quality measurement for the pump source beam at 2.07 μm after focusing with a 300 mm focal length lens. The beam diameter is measured at each axial position with a pyroelectric camera.

3.2 ZGP-based OPO

Most of the experiments were performed with a singly resonant plane-plane resonator with about 20 mm physical length, which was as short as practically possible. The following subsections describe the OPO components in more details. Experiments with a concave output coupler are described in Section 5.6, and length matching in Section 5.5.

3.2.1 ZGP crystal

ZGP is a positive uniaxial crystal ($n_e > n_o$). The effective nonlinear coefficients are:

- $d_{eff} = d_{36} \cdot \sin(2\theta) \cdot \cos(2\Phi)$ for type *I* phase matching *(3.1)*
- $d_{eff} = d_{36} \cdot \sin(\theta) \cdot \sin(2\Phi)$ for type *II* phase matching, *(3.2)*

where θ is the angle between the direction of propagation and the crystal z-axis, and Φ is the angle between the projection of the direction of propagation on the crystal xy-plane and the crystal x-axis. The crystal available for this work was cut for type 1 phase matching, with $\theta \approx 51°$. The pump beam has ordinary polarisation, and the signal and idler are extraordinary beams (see beam polarisations in Figure 3.2).

The optical damage threshold of ZGP is reported to be 10 J/cm^2 for 70-200 ns pulses and 4.5 J/cm^2 for 150 ps pulses (30 GW/cm^2) [9, 10]. In a recent work, damage was found to occur at 3.5 J/cm^2 in 100 ns pulses [11]. However, the limiting factor is often the damage threshold of the AR-coating, which is more on the order of 1 J/cm^2. For this reason, we limited the maximum fluence to 1 J/cm^2 in the experiments.

The ZGP crystal used in this work is 15 mm long and AR-coated for 2.1 μm and 3-5 μm (it was purchased from *INRAD* in January 2000). Figure 3.4 shows the measured optical transmission of the ZGP crystal. The blue solid line shows the transmission of the coated 15 mm long crystal measured in our lab. Owing to problems with calibration of the absolute level in the transmission measurements, the curve has been adjusted to 97.2% transmission at 4.1 μm. This value corresponds to perfect AR-coating and the same absorption as in an uncoated crystal measured by *INRAD* [12] and showed by the red dotted curve in Figure 3.4. The black dashed line shows the Fresnel losses of an uncoated ZGP crystal.

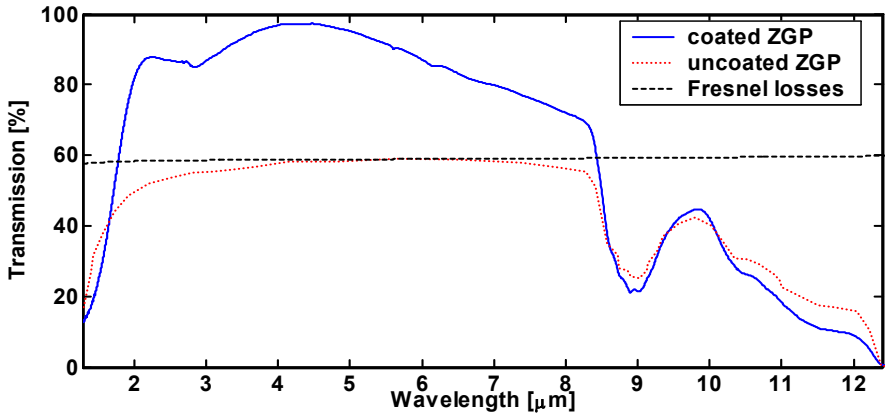

Figure 3.4. Measured optical transmission of ZGP crystal. The blue solid and red dotted lines show transmission for 15 mm long coated (measured by us) and 14 mm long uncoated crystals (measured by INRAD), respectively. The black dashed line shows the Fresnel losses of an uncoated ZGP crystal (i.e. two ZGP-air interfaces).

The absorption coefficient of the 15 mm long ZGP crystal shown in Figure 3.5(a) is derived from the transmission for the uncoated ZGP and the Fresnel losses in Figure 3.4. The spectral reflectance of the AR coating (Figure 3.5(b)) is derived from the transmission for the coated and uncoated ZGP and the Fresnel losses. The dip in transmission around 9 μm in Figure 3.4 is assigned entirely to absorption in ZGP. As a result, the estimated absorption coefficient at 9 μm is as high as 80 m^{-1}, which is in good agreement with measurements made by *INRAD* [12] and in other works [13-15]. It is not clear whether this value varies from sample to sample. In the simulations of the ZGP-based OPO presented later, we used the estimated ZGP absorption coefficient and coating reflectance shown in Figure 3.5.

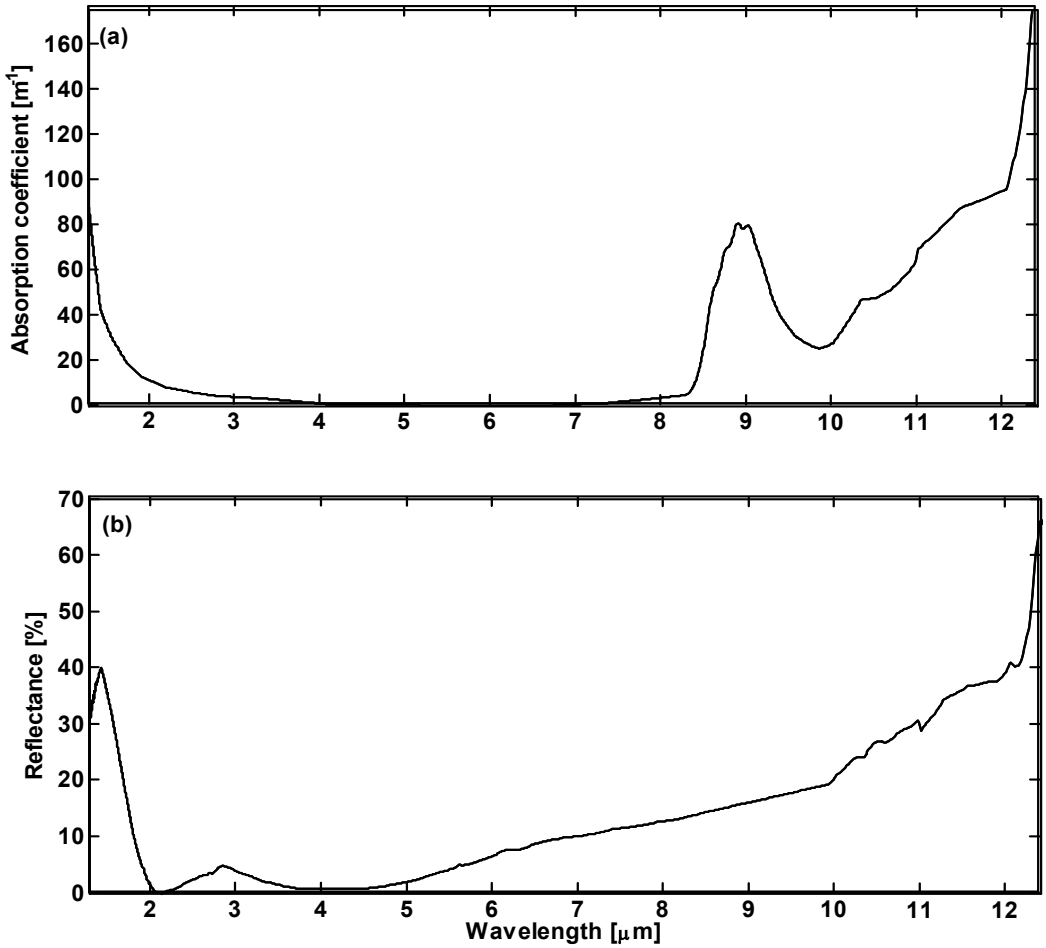

Figure 3.5. (a) Estimated ZGP absorption coefficient. (b) Estimated ZGP crystal AR-coating reflectance for one surface.

3.2.2 OPO mirrors

The OPO input and output mirrors M_1 and M_2 are identical. They were purchased from *QUALITY THIN FILMS, INC (QTF)* with the following coating specifications:

Main coating: 95%R @ 2.6-2.8μm / HT @ 2.1 & 8-10μm.
AR-coating: AR @ 2.1 & 8-10μm

Figure 3.6 and Figure 3.7 show the main coating transmission and AR-coating reflectance curves delivered by *QTF* together with the mirrors. The AR-coating reflectance varies from 1.5 to 9.5% in the 8-10 μm range, which is poorer than expected.

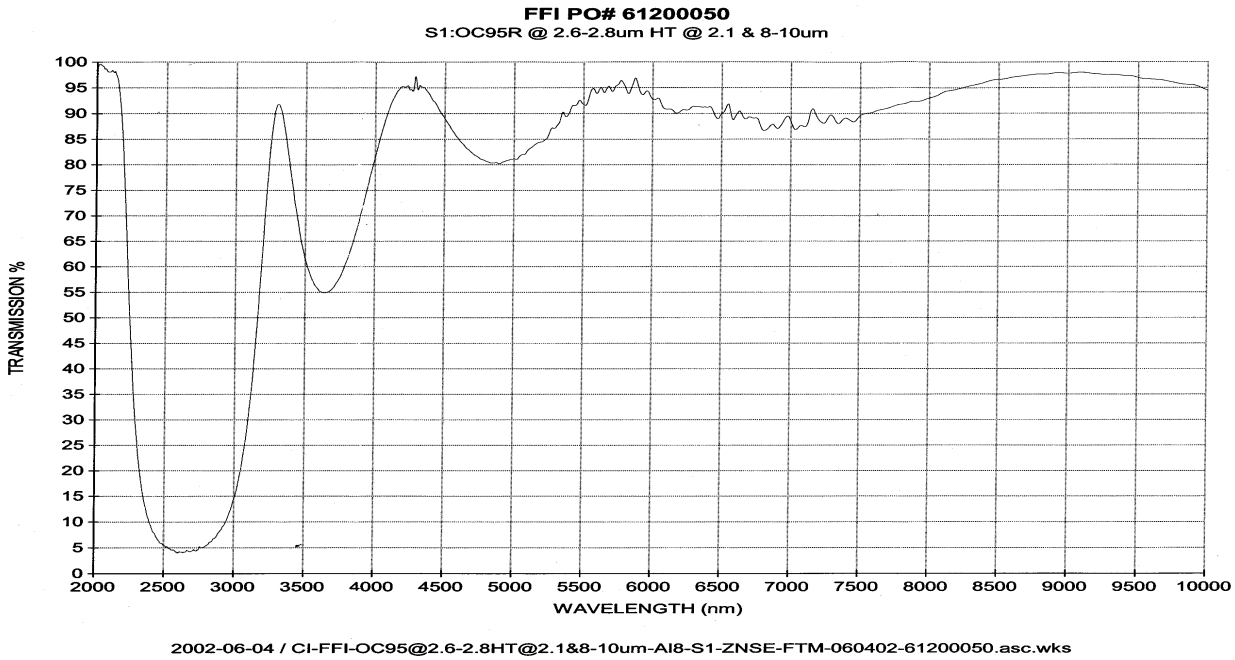

Figure 3.6. Mirror main coating transmission measured by QTF.

Figure 3.7. Mirror AR-coating reflectance measured by QTF.

Figure 3.8 shows the measured total transmission of the OPO mirrors. The critical values are also summarized in Table 3.1.

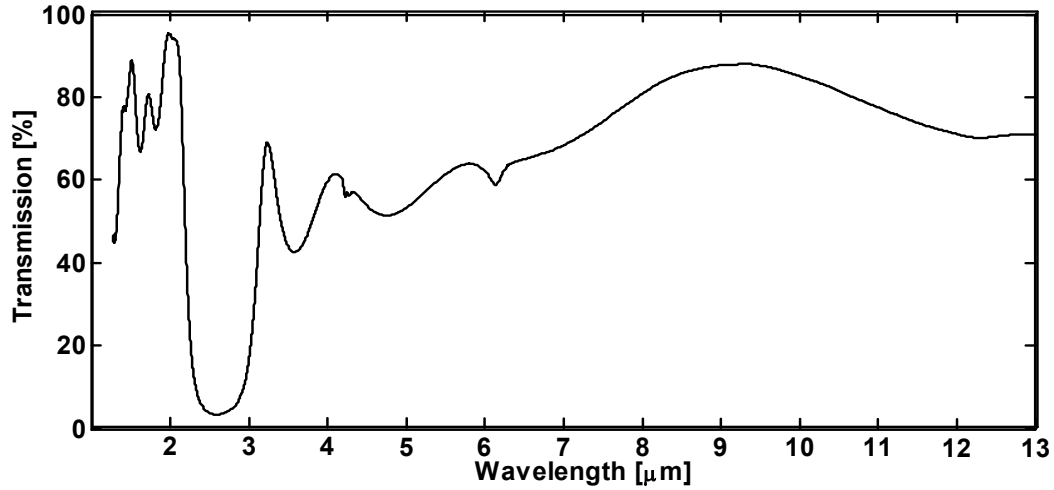

Figure 3.8. Mirror transmission measured by us.

Beam	Main coating transmission (specified by QTF)	AR-coating reflectance (specified by QTF)	Total mirror transmission (measured by us)
Pump (2.07μm)	99%	0.5%	94%
Signal (2.6-2.8μm)	4-6%	7.5-9.8%	3.5–5%
Idler (8μm)	92%	9.8%	81%
Idler (9μm)	98%	4%	88%
Idler (10μm)	95%	1.6%	85%

Table 3.1. Main coating transmission, AR-coating reflectance and total transmission of the OPO mirror.

At the idler wavelengths, we measured lower transmission than expected from the *QTF* data.

The roundtrip loss is defined by the following equation.

$$L_{RT} = 1 - r_{mirror}^2 \cdot T_{ZGP}^2 \tag{3.3}$$

where r_{mirror} is the mirrors reflectance and T_{ZGP} is the transmittance of the coated ZGP crystal.

The roundtrip loss is calculated to be about 32% at 2.7 μm and >99.6% in the 8-11 μm range. We thus conclude that the OPO is singly resonant (SRO), which means that only the pump and signal are incident on the crystal and that the idler can adapt its phase to maximise the gain.

3.2.3 OPO wavelength tuning

The signal, idler and pump frequencies ω_1, ω_2 and ω_3 are related to each other by the energy conservation law:

$$\omega_3 = \omega_1 + \omega_2 \tag{3.4}$$

Figure 3.9 shows the generated signal (2.5 - 2.8 µm) and idler (8 - 12 µm) wavelengths when the OPO is pumped at 2.073 µm.

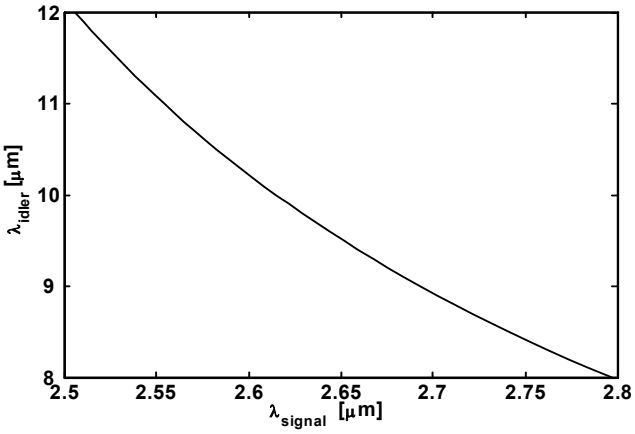

Figure 3.9. Signal and idler wavelengths for an OPO pumped at 2.073 µm.

Wavelength tuning is achieved by rotating the ZGP crystal. According to the type I phase matching curve for ZGP, two pairs of signal and idler wavelengths can be generated for a given crystal tuning-angle, as shown by Figure 3.10. The two beams at $\lambda < 4$ µm are called "signal" beams and the two beams at $\lambda > 4$ µm are called "idler" beams. We denote this type of multiple signal and idler emissions for *dual signal/idler wavelength operation* or more generally for *dual phase matching operation*. The two idler wavelengths are designated as the "short" and the "long" idler wavelengths.

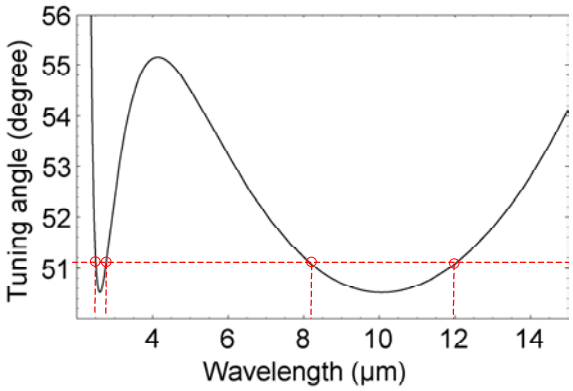

Figure 3.10. Phase matching in ZGP with 2.07 µm pump, based on Sellmeier equations of Barnes et al. [16].

The filter F_1 after the OPO (see Figure 3.1) is a long-pass filter (*LP-6000* filter from Spectrogon) transmitting the idler beam (84 to 92% transmission in the 8-12 µm range) and rejecting the signal and the pump beams (see Figure 3.11).

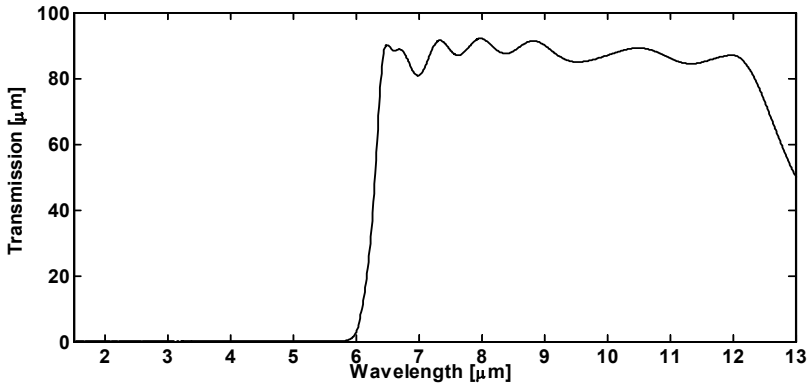

Figure 3.11. LP-6000 filter spectral transmission.

3.3 Monochromator for spectral measurements

The ZGP OPO output beam is focused into the monochromator (*CVI Digikrom 240*) by two ZnSe lenses (L_1 and L_2) via two flat gold mirrors, M_{b1} and M_{b2} as shown in Figure 3.1. The 75 g/mm grating used in the monochromator has maximum efficiency at 8 μm and an efficiency between 97% and 60% in the 8-12 μm spectral range (beam polarized perpendicular to the grooves). We use monochromator slit sizes of 300 or 500 μm, which correspond to spectral resolutions of 8 and 14 nm, respectively. As we shall see later, the spectral width of the idler and the signal is much larger than the monochromator spectral resolution with these slits. The monochromator is calibrated at 2.128 μm (2nd order of the Nd:YAG laser beam at 1.064 μm). The wavelength of the pump source was measured to be 2.073 μm.

3.4 Beam quality measurements

M_{al} is an aluminium mirror used to direct the beam towards the pyroelectric camera (*Spiricon Pyrocam 3*) for beam shape and beam quality measurements, as illustrated by Figure 3.12. The lens L_4 focuses the idler beam to a waist, and the beam shapes are recorded at different positions of the camera before and after the beam waist to measure the beam quality.

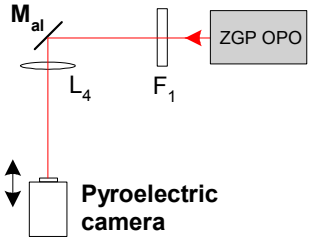

Figure 3.12. Set-up for beam quality measurements.

4 SIMULATION MODEL

Numerical simulations were performed with the simulation program *SISYFOS* developed at FFI and described elsewhere [17, 18]. This chapter presents the simulation model and parameters. The numerical simulations are compared to the experimental results in Chapter 5.

The pump beam used in the simulations has an asymmetric Gaussian temporal profile with 10 ns rise time and 15 ns fall time (measured to half maximum) and 100 GHz spectral bandwidth. The spectral width of the pump is modelled by multiple longitudinal modes with random phases and random amplitudes with a Gaussian distribution. Spatially, the pump beam is assumed to be Gaussian with a $1/e^2$ diameter of 800 μm (the pump energy is limited to 2 mJ/pulse at 2.073 μm in consideration of the optical damage threshold). The ZGP crystal is 15 mm long and the d_{36} non-linear coefficient is taken to be 75 pm/V [14]. The modelled system is sketched in Figure 4.1. The gap_1 and gap_2 gaps are equal to 3 and 2 mm, respectively.

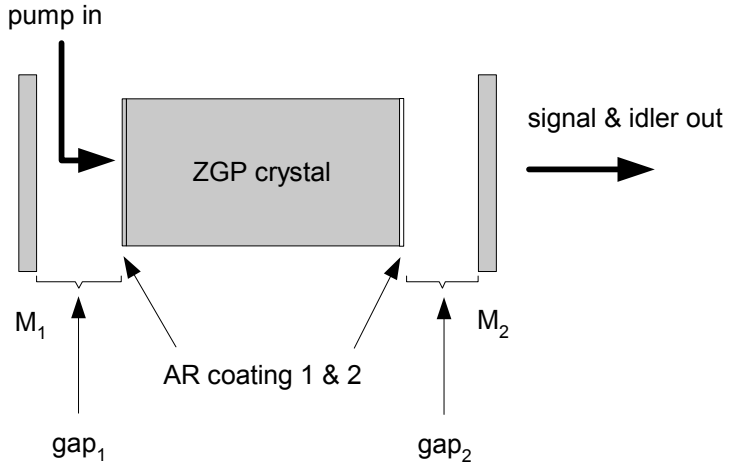

Figure 4.1. ZGP OPO simulation model.

The signal and idler spectra of the ZGP-based OPO can be very broad (see Figure 3.10). For this reason, the spectral dependency of the coupling mirrors M_1 and M_2, the crystal absorption and the crystal AR-coatings were included in the simulation model (refer to Figure 3.8 and Figure 3.5(a-b), respectively).

Wide spectra require high temporal resolution, which makes the simulations very time-consuming. Therefore, SYSIFOS has the option to simulate a sequence of short time slices that do not cover the time axis completely. This allows high temporal resolution within each slice without making the total number of samples too large.
When these slices are spaced by one resonator round trip time, so that they represent the same part of the signal in consecutive round trips, they allow a correct reproduction of the OPO dynamics. If the time slices cover $1/n^{th}$ of the time, this approach is equivalent to including every n^{th} longitudinal mode of the resonator. The signal between two slices is

implicitly assumed to be a periodic repetition of the preceding slice. This is a good approximation as long as the pump does not vary too much during one round trip, but with a multi-longitudinal-mode pump it would lead to large fluctuations in the pump energy. To avoid this, the part of the pump pulse that is actually used in the simulation, is scaled to have the correct energy. In the simulations, we used 256 temporal sample points on a slice that was 1/40 to 1/25 of the round trip time. The beams are modelled by a 16 x 16 transverse spatial array with 120 μm pixel size. We verified the validity of the simulations with these parameters by comparing with simulations with higher time and space resolution.
Note that all simulations are based on Sellmeier equations of Barnes et al. [16], which seem to fit our experimental results best (see Figure 5.6).

5 EXPERIMENTAL RESULTS AND COMPARISON WITH SIMULATIONS

The maximum pump energy was 2 mJ/pulse in order to limit the pump beam peak fluence in the ZGP crystal to ≈ 0.8 J/cm^2. Note that the total fluence (sum of the pump, idler and signal fluence) is significantly higher. The signal fluence gives the main contribution to the total fluence due to low signal out-coupling (a few percent). It is expected to be higher when the idler is tuned to long idler wavelengths because the signal output coupling drops from 5% at 2.7 μm (λ_i = 8 μm) to 3.6% at 2.55 μm (λ_i = 10 μm) and also because the photon energy of the signal increases. Simulations indicate that the peak total fluence on the ZGP crystal faces increases from 2.0 J/cm^2 to 2.9 J/cm^2 when the idler wavelength is tuned from 8 to 10 μm. This later fluence turned out to be too high for the AR-coating, and a small damage to the occurred when the OPO was tuned to longer idler wavelengths.

In the following experiments, we used the 20 mm long linear resonator described in Section 3.2.

5.1 Nitrogen flushing

Once the optical system was aligned and optimised, a small audible noise at the 20 Hz pulse repetition rate of the pump source was heard. H_2O and/or CO_2 absorption in the 2.5-2.8 μm signal band was suspected to cause local heating of the air that gives rise to this noise. This should be avoided since it may cause damage to the mirrors or to the ZGP crystal, and because it may cause additional resonator losses. At the time of the experiments, the temperature was about 26°C in the lab and the relative humidity was 50-60%. A simulation performed with the software *Modtran* (*Moderate Resolution Transmittance Code*) shows that very strong atmospheric absorption occurs in the 2.5-2.8 μm signal spectral region and that water vapour is responsible for most of this absorption (see Figure 5.1).

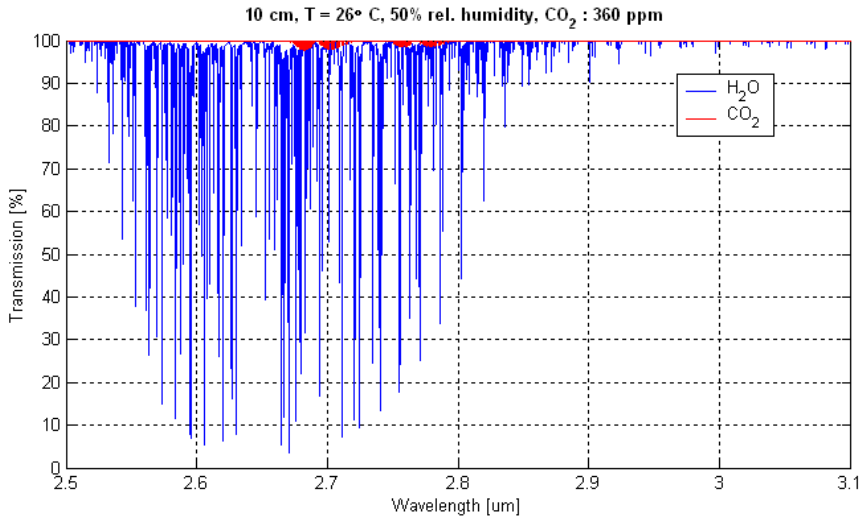

Figure 5.1. H_2O transmission with 50% relative humidity (blue curve) and CO_2 transmission with 360 ppm CO_2 (red curve) through 10 cm atmosphere, at 26 °C.

Absorption can be reduced by lowering the water vapour content in the volume that surrounds the OPO. A box was built around the OPO and the relative humidity was decreased by flushing with N_2. The box was built so that it would allow adjusting the mirrors and tuning the crystal. It was not sealed since it had two apertures for the incoming pump beam and the output idler beam. Nevertheless, we reached less than 6% relative humidity in the box by continually flushing with nitrogen. The absorption and, consequently, the audible noise disappeared when flushing. We did not, however, observe any higher signal energy. We also attempted to use Si-gel crystals instead of nitrogen flushing. Such crystals absorb water vapour and thus reduce humidity. We reached 20-30% relative humidity in the box by using Si-gel, which was much higher than the <6% we got with N_2 flushing. The ZGP OPO was therefore flushed with N_2 in the rest of the experiments.

5.2 Performance at 8 μm idler wavelength

5.2.1 Idler output energy

The measured and simulated I/O curve is shown in Figure 5.2. In the experiment, we obtained 180 μJ at 8 μm idler wavelength with 2 mJ pump energy incident on the incoupling mirror of the OPO, which corresponds to 9% energy conversion efficiency to the idler and 35% photon conversion efficiency. The pump threshold was measured to be about 270 μJ. The simulations predict a lower threshold, which may indicate a slight misalignment of our OPO. The simulations accounted for the crystal absorption, AR-coating losses and OPO mirrors reflectance. Simulations with collinear phase matching (blue triangles) show a roll-off at high energy because of back-conversion. Simulations with 7 mrad non-collinear phase matching (red triangles) give better conversion efficiency, and are in very good agreement with the experimental data. Improved conversion efficiency with non-collinear phase matching has also been reported previously [6, 19]. Note that the OPO resonator was adjusted to get the best conversion efficiency at high energy and was therefore likely to be slightly non-collinear, as suggested by the present simulations.

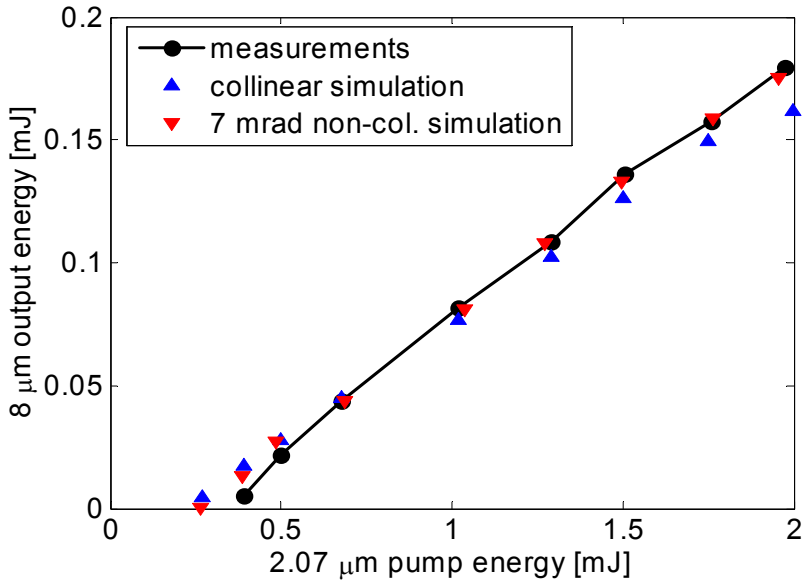

Figure 5.2. Measured and simulated idler output energy at 8 μm as a function of pump energy, with 20 mm mirror separation. Note that the non-collinear phase matching angle refers to the angle between the pump and the signal inside the ZGP crystal..

5.2.2 Beam quality

The beam quality was measured by focusing the idler beam to a waist and taking series of images at different axial positions z, as discussed in Section 3.4. The diameter 2ω of the beam profile is measured for each of those images by approximating each profile with a Gaussian. Figure 5.3 shows a plot of those measurements in both horizontal (non-critical) and vertical (critical) directions. Beam quality is derived by fitting the following function, describing the axial evolution of the beam radius $\omega(z)$, with the measured data.

$$\omega(z) = \omega_0 \left[1 + \left(M^2 \cdot \frac{z - z_w}{z_0} \right)^2 \right]^{\frac{1}{2}} \tag{5.1}$$

where ω_0 is the beam radius at the waist position z_w, z_0 is the Rayleigh distance and M^2 is the beam quality.

The beam quality was found to be 3.0 in the non-critical and 2.4 in the critical direction. The waist positions and radius as well as the beam quality M^2 are different in the horizontal and vertical directions. Figure 5.4 shows an example of the idler beam.

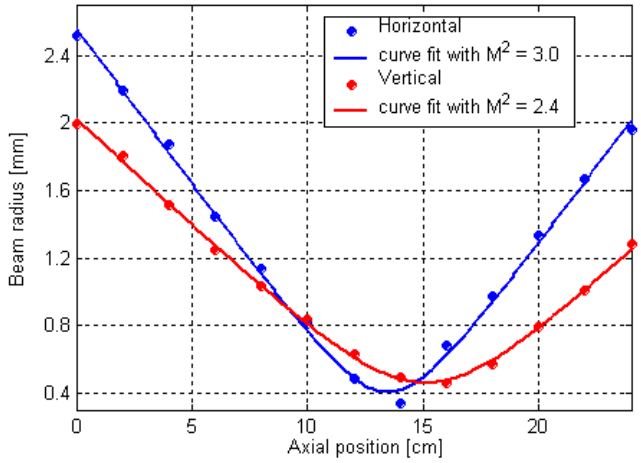

Figure 5.3. Beam quality measurement for the ZGP-based OPO tuned to 8 µm idler wavelength, after focusing with a 300 mm focal length lens.

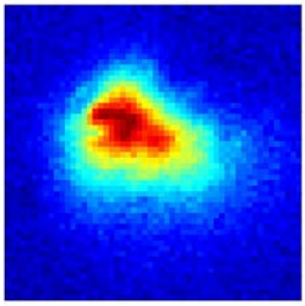

Figure 5.4. Idler beam shape at 8 µm after focusing with a 300 mm focal length lens, in axial position $z \approx 380$ mm.

5.2.3 Pulses shapes

Figure 5.5 shows the incoming and depleted pump pulse shapes at 1.97 mJ pump energy and the idler pulse at 8 µm. The pulse lengths are 27 and 25 ns (FWHM) for the incoming pump and the idler, respectively. Note that the pulse measurements were not taken simultaneously and were therefore not synchronised. We used the infrared detector *VIGO* PD-10.6-5. The position of the measured idler pulse on the time axis is determined by comparison with the theoretical idler pulse (i.e. the energy normalised difference between the incoming and depleted pulse).

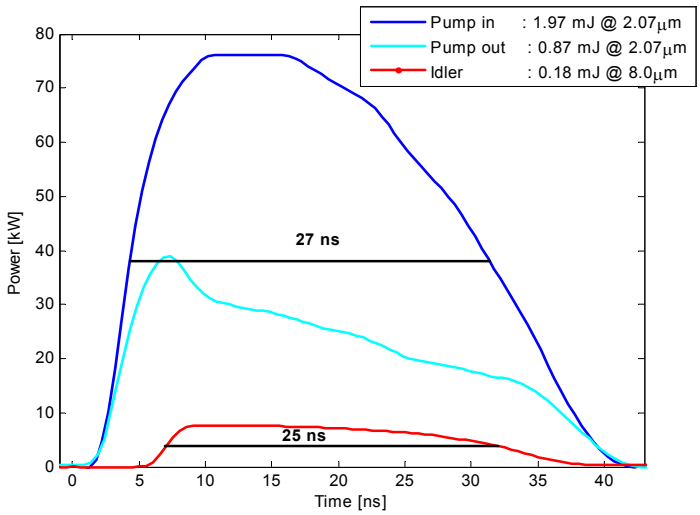

Figure 5.5. Pump and idler pulses. The blue solid line shows the incoming pump pulse at 1.97 mJ pump energy, the light blue line is the depleted pump pulse after the OPO, and the red line is the idler pulse at 8 μm.

5.3 Phase matching / Tuning

In Figure 5.6, we show how the measured idler wavelength varies as a function of internal angle with respect to the ZGP optical axis, and we compare it to calculations based on different published Sellmeier equations according to references [16, 20-23]. In the measurements, the idler wavelength was defined as the centre wavelength of the broadband emission. The exact vertical position of our tuning curve is uncertain, as the exact cutting angle was not known from the crystal manufacturer (*INRAD* originally stated 53° but this was obviously wrong). In Figure 5.6, we have assumed the cutting angle to be 51.65˚. We experimentally observed dual signal/idler wavelengths in the 9-11 μm range as illustrated in Figure 3.10.

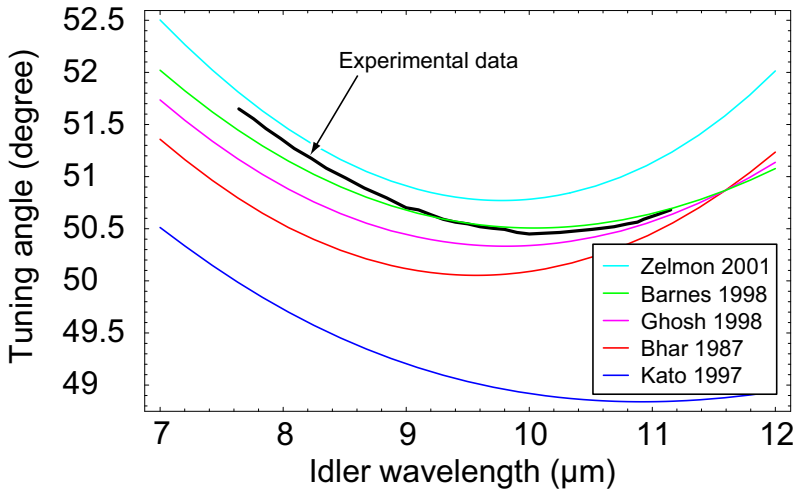

Figure 5.6. Comparison between experimental and theoretical phase-matching curves based on different Sellmeier equations according to references [16, 20-23].

5.4 Wavelength tuning

5.4.1 Output spectra

The output wavelength of the OPO is tuned by adjusting the angle of the ZGP crystal as explained in Figure 3.10 and measured in Figure 5.6. Figure 5.7 shows the measured and simulated spectral output at different tuning angles, which illustrates dual phase matching operation from 8 μm to the degeneracy wavelength at 10 μm. The red dashed lines show the corresponding phase matched idler wavelengths according to the Sellmeier equations of Barnes et al. [16]. Also shown is the single-pass signal gain given by

$$G = \cosh^2(gL) + \left(\frac{\Delta k}{2|g|}\right)^2 \sinh^2(gL) \tag{5.2}$$

where L is the length of the non-linear crystal, $\Delta k = k_3 - k_2 - k_1$ is the phase mismatch, and g is the small signal coefficient :

$$g = \sqrt{\eta^2 N_3 - \left(\frac{\Delta k}{2}\right)^2} \ . \tag{5.3}$$

Here, N_3 is the pump intensity in units of $photons \cdot s^{-1} \cdot m^{-2}$ and η^2 is the small signal gain factor in the coupled wave equations,

$$\eta^2 = d_{eff}^2 \cdot \frac{2\hbar\omega_1\omega_2\omega_3}{n_1 n_2 n_3 c^3 \varepsilon_0} \ , \tag{5.4}$$

where ω_i and n_i are the angular frequency and refractive index of beam i, respectively, d_{eff} is the effective non-linearity for the phase matched process (see Equation 3.1) and c, $\hbar$ and ε_0 are the speed of light, the Planck constant ($\hbar = h/2\pi$), and the permittivity of vacuum, respectively. The pump peak fluence for the single-pass gain was taken to be 0.8 J/cm^2.

The measured spectra fit well with the single-pass gain curve. The simulated spectra with 2 mJ pump energy match also quite well with the gain curve in Figure 5.7(a-c) and (e) but are broader than the measured spectra at 8, 8.5 and 9 μm short idler wavelengths. Note the discrepancy of the simulated spectrum with 2 mJ pump energy at θ = 50.55° tuning angle as shown in Figure 5.7(d). The comparison between the simulated spectra at 0.6 mJ (about three times the OPO energy threshold) and 2 mJ pump energy shows that the spectral mismatch arises with high pump energy. We have previously studied how the spectrum of an OPO can broaden strongly at high pump energy [24], but the question is why this seems to happen only in the simulations. Figure 5.2 shows that the measured threshold is higher than the simulated threshold. This can indicate that the simulation is driven further into the nonlinear regime than the experimental device. It is possible that the deviation of the spectrum from the gain curve in

Figure 5.7(d) is a real effect that could also have been measured if we could pump the OPO harder. Tests with various settings for resolution and tolerance parameters gave no evidence for numerical problems, but we cannot rule out the possibility that the spectral deviation is a simulation problem that appears in the highly nonlinear regime.

In Appendix A, we present further simulations with SLM pump, SRO OPO and ideal crystal and study the impact on the spectral output.

Dual phase matching operation was predicted by the simulations, but was not observed experimentally for idler wavelengths at 8 and 8.5 μm (see Figure 5.7(a-b)), possibly because the power of longer idler wavelength was lower than expected and too weak to be detected (the grating efficiency decreases with the wavelength in the 9-12 μm range). We measured instead the spectra of the signal in the 2.45-2.85 μm band and revealed a second wavelength at those angles, as shown by Figure 5.8. A possible explanation for the very low intensity of the idler long wavelength is that the beams in the experimental OPO were not exactly collinear, as suggested by the non-collinear phase matching simulations (see Appendix B). As the non-collinear phase matching angle increases, the simulations indicate that the intensity of the long idler wavelength drops off (see Figure B.1) and the simulated conversion efficiency reaches that of the measurements (see Figure 5.2). It may also be possible that the simulations overestimate the power of the long idler wavelength. The reason for this may be that we used a fixed value for d_{eff} for the whole frequency range in the simulations. Miller's rule predicts only a small variation, but this rule may break down for the long wavelengths that experience significant absorption. Thus, the real d_{eff} for the long wavelengths may be smaller than we assumed.

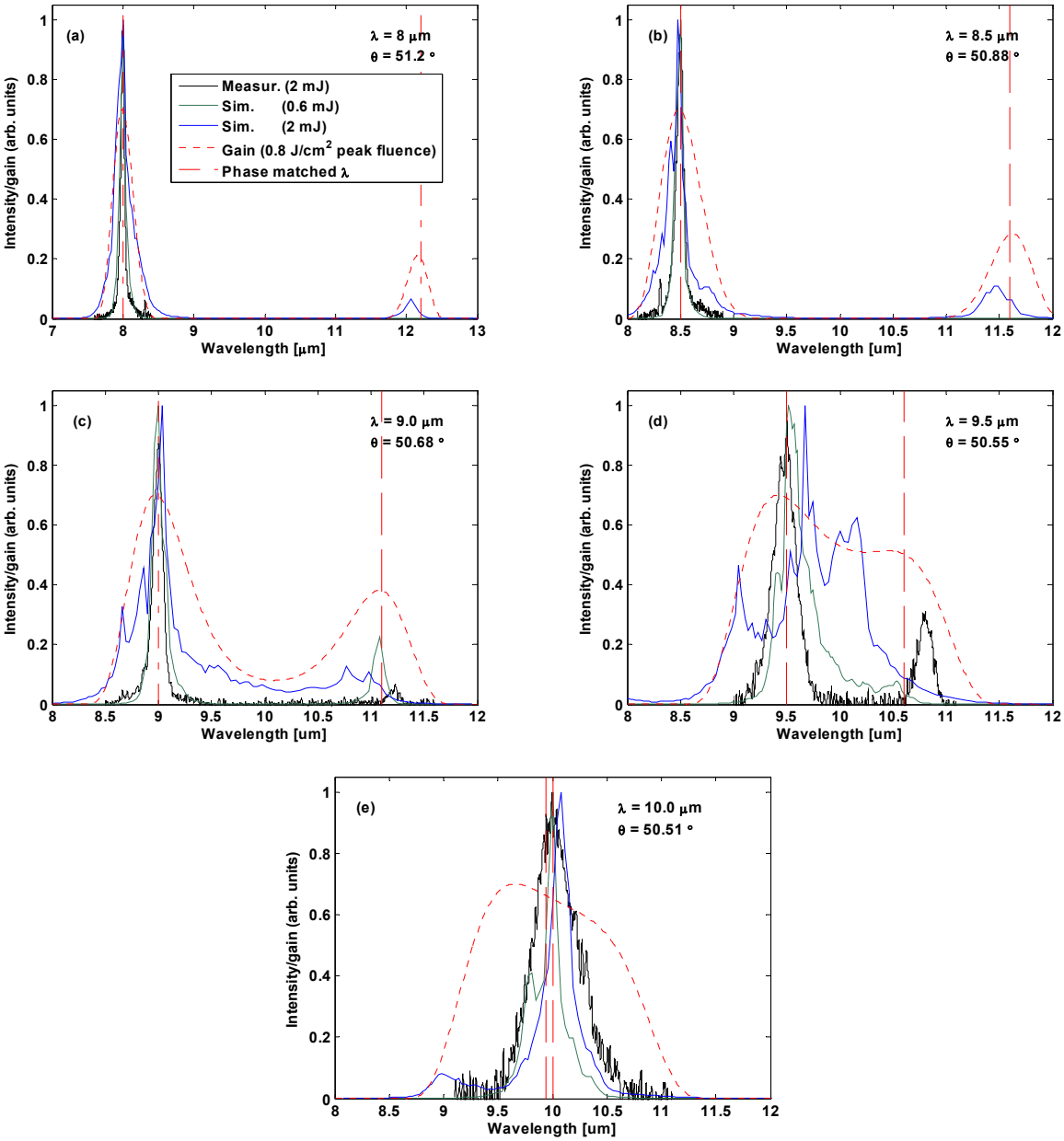

Figure 5.7. Measured and simulated idler spectra at different tuning angles, for 2 mJ pump energy. The simulated spectra are based on five-runs average. The dotted line shows the single-pass signal gain for 0.8 J/cm^2 pump peak fluence.

The measured spectral widths (FWHM) are summarized in *Table 5.1*.

Wavelength [μm]	FWHM [nm]
7.98	68
8.48	86
8.98 / 11.21	113 / 113
9.48 / 10.78	261 / 182
9.58 / 10.67	373 / 300
10.0	506

Table 5.1. Measured spectral width of the idler beams at different wavelengths.

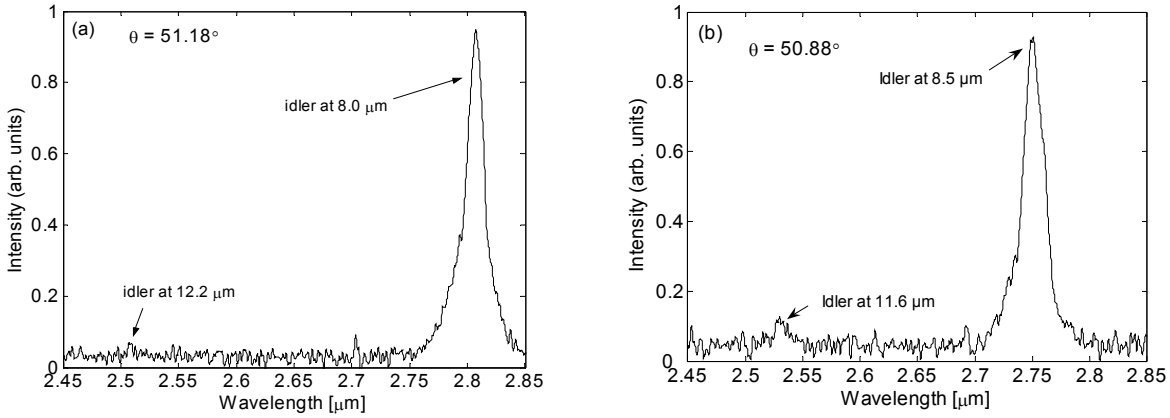

Figure 5.8. Measurements of dual signal wavelength operations at $\theta = 51.18°$ and $\theta = 50.88°$. The corresponding dual idler wavelengths are also indicated. Note that the 2.5-2.8 μm spectral band is subject to strong absorption lines in the lab atmosphere, as shown in Figure 5.1 (not visible because not resolved by the spectrometer).

5.4.2 Conversion efficiency

As the OPO is tuned to longer wavelengths, poorer conversion efficiency is to be expected due to increasing crystal absorption coefficient and poorer AR coating[*]. Also, the output spectral bandwidth gets larger. The energy conversion efficiency decreases from 9% to 0.7% when the wavelength increases from 8 to 11 μm, as shown in Figure 5.9. We observe a plateau at about 3 % efficiency in the 9-10 μm range. Simulations were also performed for comparison (see blue circles in Figure 5.9).

Conversion efficiency calculations are not straightforward because of dual phase matching operation. We used the measured and simulated output spectra shown in Figure 5.7 to calculate the energy partition into the short and long idler wavelengths (defined as the centre wavelengths of the broadband emission). Note that this method is not very accurate for the simulations as the spectra of the short and long idler broaden and overlap while tuning the OPO towards "idler degeneracy".

[*] In fact, according to Equations (5.2-4), the gain also becomes smaller (about 10% from 8 μm to 11 μm), but this is neglectable in comparison with the increased losses.

Simulated and measured conversion efficiency agree rather well even though there was a spectral discrepancy at the tuning angle $\theta = 50.55°$ (corresponding to $\lambda = 9.5$ µm phase matched wavelength), as discussed earlier in Section 5.4.1.

The AR-coating of the ZGP crystal is optimal for use in the 3-5 µm range (less than 4% reflectance) and is significantly poorer in the 8-12 µm range (13 to 40% reflectance), as can been seen in Figure 3.5(b). Simulations assuming ideal AR-coatings (0% reflectance at pump, signal and idler) and ideal OPO mirrors (100% transmission at pump and idler and 96% reflectance at signal) predict only slightly higher conversion efficiency at the short idler wavelengths (i.e. 10.5% at 8 µm) but much better efficiency at the long idler wavelengths around 12 µm, where the crystal coating reflectance increases so drastically (see red triangles in Figure 5.9).

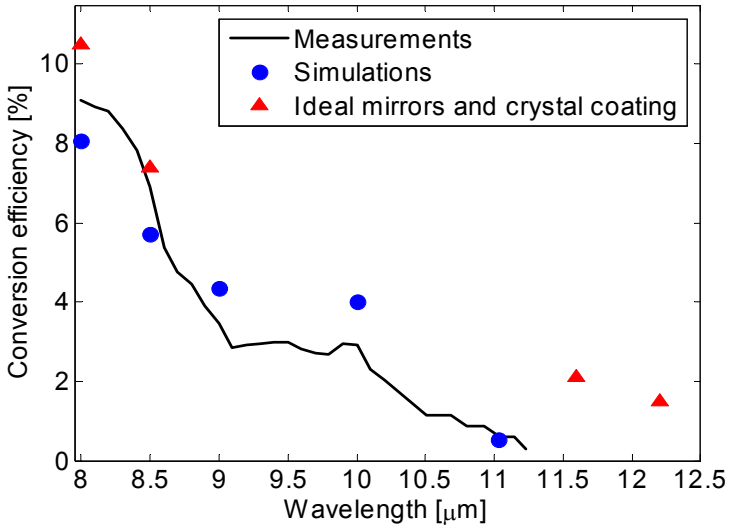

Figure 5.9. Conversion efficiency versus wavelength with 2 mJ pump. The black solid line shows the experimental measurements and the blue circles the simulation data. The red triangles show simulations assuming ideal OPO mirrors (100% transmission at idler and pump and 94% reflectance at signal) and ideal crystal AR-coatings (0% reflectance at pump, signal and idler).

5.5 Length matching experiment

We refer to Section 2.2 for length matching theory and references to previous work. Our experiment is illustrated in Figure 5.10 where a ZGP-based SRO tuned to 8 µm wavelength output is pumped by a MLM pump source. The SRO output energy is measured for different positions of the mirror M_2, i.e. for different resonator optical lengths.

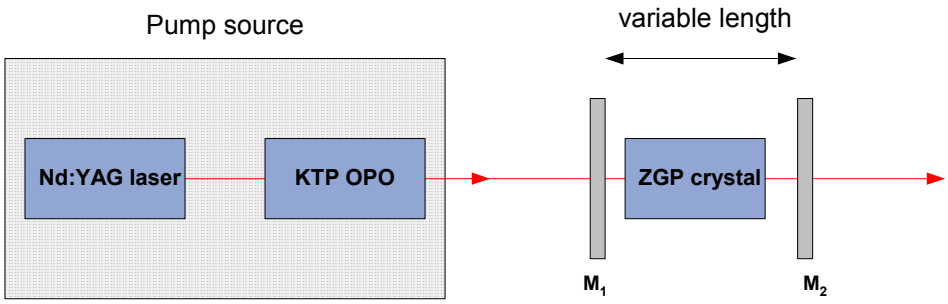

Figure 5.10. Setup of length matching experiment.

The overall trend is that the conversion efficiency decreases as the mirror separation of the OPO increases, as a result of a longer build-up time leading to larger threshold. However, the energy has a peak at 49 mm OPO mirror separation, which corresponds to the optical resonator length of the pump source. Nevertheless, since the resonator length needed to match the length of the KTP-based OPO was much longer than the smallest possible length for the ZGP OPO, and because the length matching effect for singly resonant OPOs is significantly smaller than for doubly resonant OPOs, the output energy at the shortest resonator length was the highest, as can be seen in Figure 5.11.

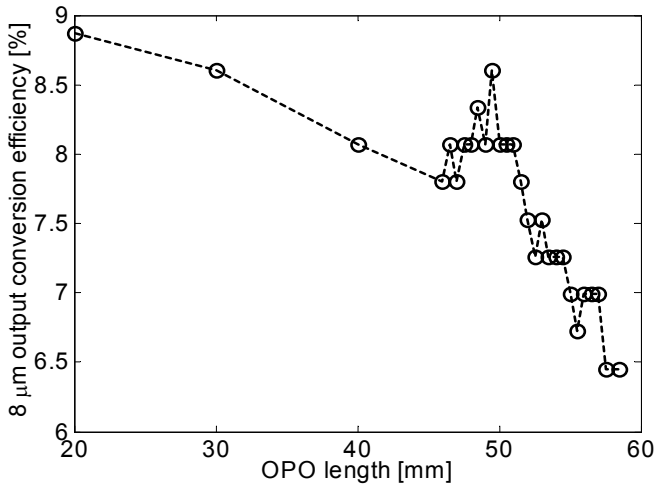

Figure 5.11. Conversion efficiency at 8 μm for the ZGP OPO as a function of resonator length for 2 mJ pump energy.

5.6 Performance with concave output coupler

In this section, the plane output-coupling mirror of the OPO is substituted by a spherical mirror of 0.5 m curvature with the same coating, giving a stable resonator mode. The resonator mode size was ~ 0.5 mm ($1/e^2$ diameter).

5.6.1 Idler output power

The measured and simulated output energy data are compared for both plane and curved output coupler, as shown in Figure 5.12. The measured idler energy is similar for plane and curved output coupler. The simulations do not match with the measurements at energy above

1 mJ, and seem to indicate back-conversion in this region. As mentioned in Section 5.2.1, the OPO resonator was adjusted to get the best conversion efficiency at high pump energy and was therefore most likely non-collinear. However, further non-collinear phase matching simulations did not give better conversion efficiency. We have not identified the reason for the greater deviation of the simulation in the case with a curved output coupler, but as mentioned in Section 5.4, the simulations may be driven further into the nonlinear regime than the experiments.

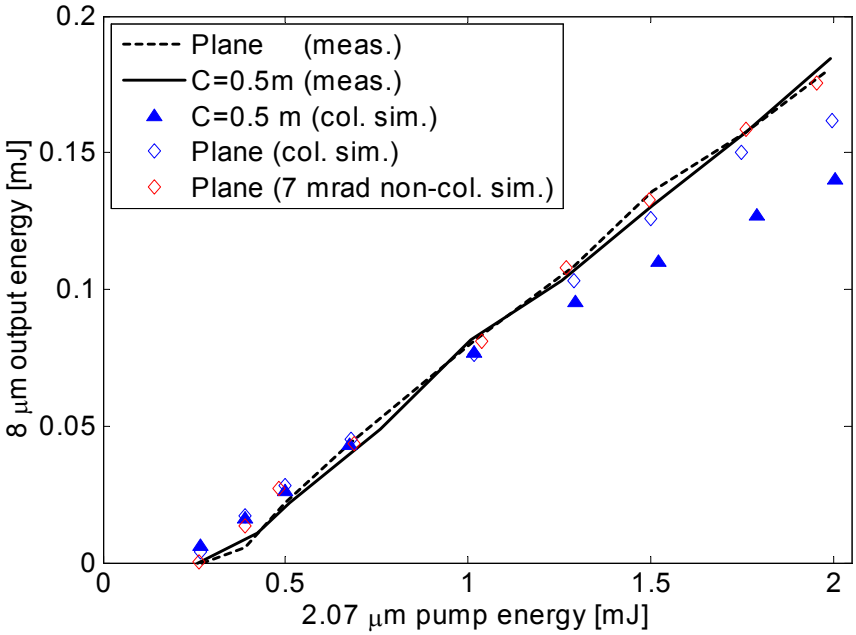

Figure 5.12. Measured and simulated idler output power at 8 μm as a function of pump energy power. The dotted and solid lines show the measurements with a plane and curved output coupler, respectively. The other symbols are explained in the legend.

5.6.2 Beam quality

The beam quality measurements are shown in Figure 5.13. The beam quality M^2 was measured to be 3.1 and 3.4 for the curved output coupler as compared to 3.0 and 2.4 for the plane output coupler, in the non-critical and critical directions, respectively. The beam quality is poorer than for the plane output coupler, although the difference is small.

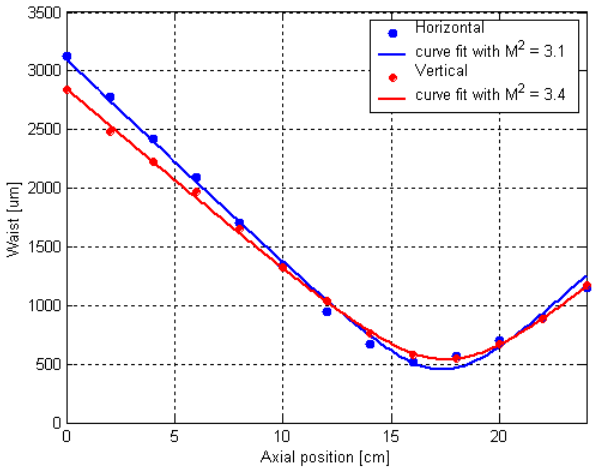

Figure 5.13. Beam quality measurement in case of spherical output coupler, after focusing with a 127 mm focal length lens.

6 CONCLUSION

We have demonstrated a low pulse rate ZGP-based OPO with wavelength tuning in the 8-11 μm range. For 8 μm idler wavelength, the threshold was 270 μJ, at 2 mJ pump energy the maximum energy conversion efficiency was 9% (i.e. 35% photon conversion efficiency), and the beam quality was measured to be $M^2 = 2.4$ and 3 in the critical and non-critical direction, respectively. Dual idler and signal wavelength operation was observed, and we found length matching effect for the singly resonant OPO. Simulations of the system have been performed, and the results are in good agreement with the experimental data in most of the cases. Some discrepancies were nevertheless observed and studied, but were not fully understood.

It can be concluded that a 2 μm pumped ZGP OPO has the potential to become an efficient high average power source in the 8 μm range when using a high pulse rate pump source. At wavelengths above 8.5 μm, absorption reduces the efficiency.

APPENDICES

A COMPARISON OF DIFFERENT SIMULATIONS

Further numerical simulations have been carried out in order to investigate the impact on the spectral output (at $\theta = 50.55°$) of modifications to the original OPO model, such as pumping with a SLM pump, the use of an "ideal" crystal (defined as having a flat spectral transmission) and the use of a singly resonant OPO (SRO). These results are gathered for comparison with the previous original OPO model in Figure A.1. The label *"i"* stands for "ideal" crystal and each spectrum is normalized and offset for easy comparison.
The total transmission of the "ideal" crystal (AR-coating included) is set to be constant over the 8-11 μm spectral range of the idler. It is chosen to be about 40%, which is the crystal transmission at 9.5 μm. The purpose is to show in which manner the spectral transmission of the crystal may influence the spectral output of the idler.
From Figure A.1, it is clear that in the case of an "ideal" crystal, the spectrum exhibits more spectral components around 9 and above 10 μm, which was to be expected (better transmission at these wavelengths than in the real crystal). In the case of SLM pump, the spectrum is modified and becomes narrower. The spectra do not coincide in any case with the phase-matched idler wavelengths shown by the dash-dotted red lines (phase matched wavelengths according Sellmeier equations).

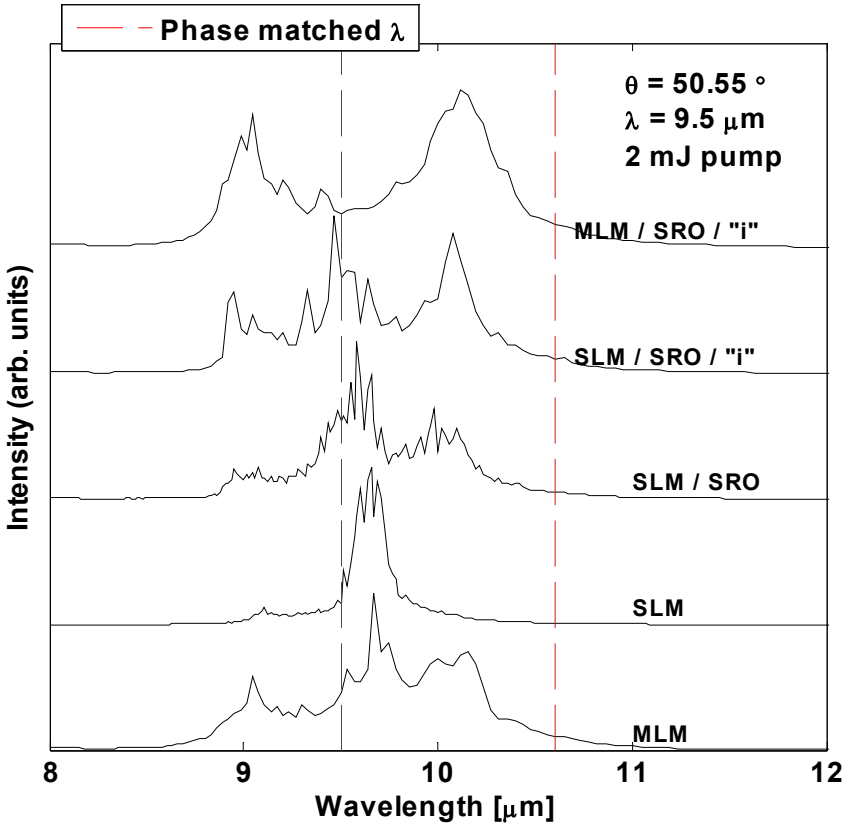

Figure A.1. Simulated idler spectral output for 2mJ pump energy and $\theta = 50.55°$ in the cases of SLM pump," ideal" crystal and SRO compared to the simulations of the original OPO (marked MLM). The simulated spectra are based on five-runs average. The dash-dotted red lines show the phase matched dual idler wavelengths in the simulations.

B NON-COLLINEAR SIMULATIONS

Non-collinear phase matching has been reported to improve conversion efficiency and to reduce threshold [6, 19]. In Section 5.2, 7 mrad non-collinear simulation gave the best conversion efficiency (see Figure 5.2). In this section, we investigate non-collinear phase matching influence of the spectral output. Figure B.1 shows idler spectra for non-collinear phase matching in the critical direction (walk-off direction) at different crystal tuning angles corresponding to idler at 8 μm and 8.5 μm. As the pump beam is tilted in relation to the OPO, non-collinear phase matching takes place and the long idler wavelength decreases in intensity, as observed in Figure B.1. The spectral widths (FWHM) did not seem to be affected by non-collinear phase matching.

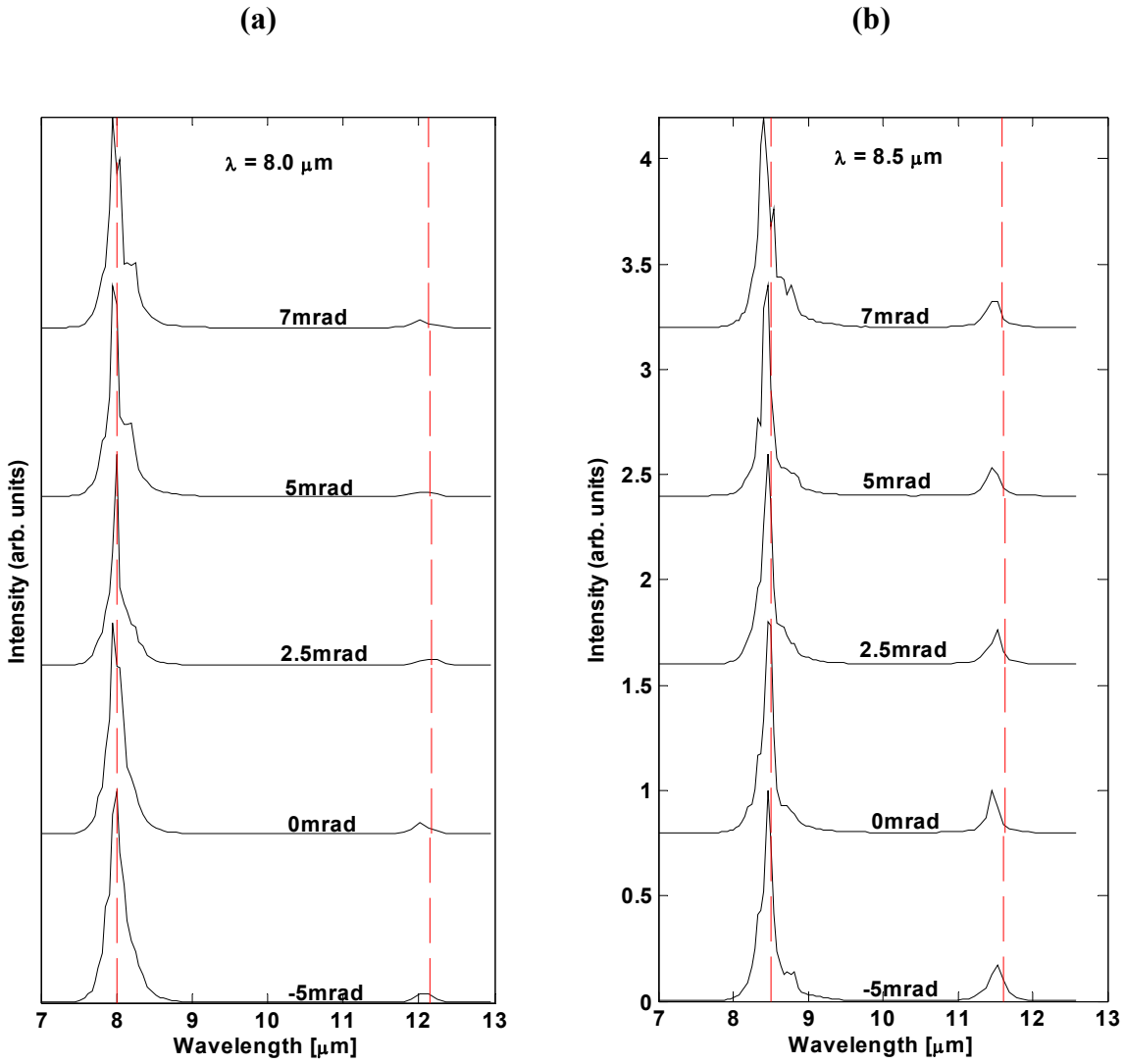

Figure B.1 *Simulated idler spectra for 2mJ pump energy and non-collinear phase matching at different angles between the pump and the signal. (a) Non-collinear phase matching in the critical direction with the short idler at 8 μm. (b) Non-collinear phase matching in the critical direction with the short idler at 8.5μm. The dash-dotted red lines show the two phase matched idler wavelengths according Sellmeier equations of Barnes et al. [16] for non-collinear phase matching. The simulated spectra are based on five-runs average.*

References

1 G Arisholm, E Lippert, G Rustad, and K Stenersen (2000). Effect of resonator length on a doubly resonant optical parametric oscillator pumped by a multilongitudinal-mode beam. *Optics Letters* **25**, 1654-1656.

2 P A Ketteridge, P A Budni, P G Schunemann, M Lemons, T M Pollak, and E P Chicklis. Tunable all solid state average power ZGP OPO. In: *Advanced Solid State Lasers*, OSA Trends in Optics and Photonics vol 19, M M Fejer, ed (Optical Society of America, Washington, DC, 1998), pp 233-235.

3 G Rustad, S Nicolas, E Lippert, K Stenersen, and G Arisholm. Tuning and dual wavelength operation of a ZGP OPO in the 8-11 micron range. In: *Advanced Solid State Photonics*, OSA Trends in Optics and Photonics vol 83, J J Zayhowski, ed (Optical Society of America, Washington, DC, 2003), pp 333-338.

4 R W Boyd. *Nonlinear Optics*. Academic Press, 1992.

5 G Arisholm (1999). *Numerical modelling of optical parametric frequency conversion and self-focusing*. Dr Scient dissertation, University of Oslo.

6 G Arisholm and G Rustad (1997). *A review of theory and materials for optical parametric oscillators in the infrared*. FFI (Norwegian Defence Research Establishment), Kjeller, Norway. FFI /RAPPORT -97/02589.

7 G Rustad, E Lippert, K Stenersen, and G Arisholm. Enhanced power from a doubly resonant optical parametric oscillator by choice of resonator length. In: *Advanced Solid State Lasers*, OSA Trends in Optics and Photonics vol 50, C Marshall, ed (Optical Society of America, Washington, DC, 2001), pp 660-665.

8 G Arisholm, E Lippert, G Rustad, and K Stenersen (2002). Efficient conversion from 1 to 2 μm by a KTP-based ring optical parametric oscillator. *Optics Letters* **27**, 1336-1338.

9 K L Vodopyanov, V G Voevodin, A I Gribenyukov, and L A Kulevskii (1987). Highly Efficient Picosecond Parametric Superluminescence in a $ZnGeP_2$ Crystal in the Range of 5-6.3 μm. *Kvantovaya Elektronika* **14**, 1815-1819.

10 R D Peterson, K L Schepler, J L Brown, and P G Schunemann (1995). Damage properties of $ZnGeP_2$ at 2 μm. *Journal of the Optical Society of America B-Optical Physics* **12**, 2142-2146.

11 K L Vodopyanov, F Ganikhanov, J P Maffetone, I Zwieback, and W Ruderman (2000). $ZnGeP_2$ optical parametric oscillator with 3.8-12.4-μm tunability. *Optics Letters* **25**, 841-843.

12 INRAD. *ZGP crystal data sheet*. http://inrad.com/pdf/Inrad_datasheet_ZGP.pdf.

13 G S Herman and G Bertelli. Far infrared spectra of nonlinear optical crystals. In: *Solid state lasers and nonlinear crystals*, SPIE Conference Proceedings vol 2379, L K Cheng, ed (SPIE, 1995), pp 291-297.

14 P D Mason, D J Jackson, and E K Gorton (1994). CO_2 laser frequency doubling in $ZnGeP_2$. *Optics Communications* **110**, 164-166.

15 P G Schunemann and T M Pollak (July 1998). Ultralow gradient HGF-grown $ZnGeP_2$ and $CdGeAs_2$ and their optical properties. *MRS Bulletin* **23**, 23-27.

16 N P Barnes, K E Murray, M G Jani, P G Schunemann, and T M Pollak (1998). $ZnGeP_2$ parametric amplifier. *Journal of the Optical Society of America B-Optical Physics* **15**, 232-238.

17 G Arisholm. Advanced numerical simulation models for second-order nonlinear interactions. In: *Fundamental Problems of Laser Optics*, Proceedings of SPIE vol 3685, N N Rosanov, ed (SPIE, Bellingham, WA, 1998), pp 86-97.

18 G Arisholm (1999). Quantum noise initiation and macroscopic fluctuations in optical parametric oscillators. *Journal of the Optical Society of America B-Optical Physics* **16**, 117-127.

19 L A W Gloster, I T Mckinnie, and T A King (1994). Noncollinear Phase-Matching in a Type-I Barium Berate Optical Parametric Oscillator. *Optics Communications* **112**, 328-332.

20 G C Bhar, L K Samanta, D K Ghosh, and S Das (1987). Tunable parametric $ZnGeP_2$ crystal oscillator. *Soviet Journal of Quantum Electronics* **17**, 860-861.

21 G Ghosh (1998). Sellmeier coefficients for the birefringence and refractive indices of $ZnGeP_2$ nonlinear crystal at different temperatures. *Applied Optics* **37**, 1205-1212.

22 K Kato (1997). Second-harmonic and sum-frequency generation in $ZnGeP_2$. *Applied Optics* **36**, 2506-2510.

23 D E Zelmon, E A Hanning, and P G Schunemann (2001). Refractive-index measurements and Sellmeier coefficients for zinc germanium phosphide from 2 to 9 μm with implications for phase matching in optical frequency-conversion devices. *Journal of the Optical Society of America B-Optical Physics* **18**, 1307-1310.

24 G Arisholm, G Rustad, and K Stenersen (2001). Importance of pump-beam group velocity for backconversion in optical parametric oscillators. *Journal of the Optical Society of America B-Optical Physics* **18**, 1882-1890.